

# Non-Normal Route to Chaos

D. Sornette\*, V.R. Saiprasad, and V. Troude

*Institute of Risk Analysis,  
Prediction and Management (Risks-X),  
Academy for Advanced Interdisciplinary Sciences,  
Southern University of Science and Technology, Shenzhen, China*  
\* *corresponding author: dsornette@ethz.ch*

Deterministic chaos is commonly associated with *spectral criticality*: exponential sensitivity is expected when Jacobian eigenvalues exceed unity in parts of the attractor, producing the local expansion that offsets contraction elsewhere. We show that this paradigm is incomplete in dimensions  $d > 1$ . We construct a bounded 3D dynamical system whose Jacobian is *pointwise spectrally contracting*, namely all instantaneous eigenvalues remain strictly inside the stability region, yet the system develops a positive maximal Lyapunov exponent and undergoes a transition to chaos as a *non-normality index* increases at fixed spectral radius. The mechanism relies on the repeated regeneration of transient non-normal amplification through endogenous switching that reinjects trajectories into amplifying non-orthogonal directions. Although demonstrated here for a discrete-time map, the mechanism is geometric and applies more broadly to deterministic dynamical systems. These results show that chaos can emerge without spectral criticality and identify non-normality as an independent route to deterministic chaos.

Deterministic dynamical systems can exhibit highly irregular behavior known as *chaos*. Since the pioneering discoveries of Lorenz, Smale, and others, chaos has been recognized as a fundamental mechanism through which simple nonlinear systems generate complex dynamics in many natural and engineered systems [1–4]. Understanding the mechanisms that generate chaos is therefore a central problem in nonlinear science. Classical routes to chaos, such as period-doubling cascades, intermittency, and quasiperiodicity, have provided deep insight into how deterministic systems lose stability and develop sensitive dependence on initial conditions [5–7]. Identifying the dynamical mechanisms that underlie chaotic behavior remains crucial both for theoretical understanding and for predicting or controlling complex dynamics in physical systems.

Chaos in deterministic dynamical systems  $\mathbf{x}_{n+1} = \mathbf{f}(\mathbf{x}_n)$  with  $\mathbf{x}_n \in \mathbb{R}^d$  is commonly diagnosed by a positive maximal Lyapunov exponent, which measures the average exponential separation of nearby trajectories and reflects sensitive dependence on initial conditions [8, 9]. In one dimension, and more generally when the Jacobians  $\mathbf{Df}(\mathbf{x})$  are *normal* (i.e., matrices that commute with their conjugate transpose), the growth of perturbations is tightly controlled by the instantaneous eigenvalues. Indeed, for normal Jacobians the  $L_2$  operator norm equals the spectral radius,  $\|\mathbf{Df}(\mathbf{x})\|_2 = \rho(\mathbf{Df}(\mathbf{x}))$ . As a result, a positive maximal Lyapunov exponent requires that the map be locally expansive along sufficiently many portions of the trajectory. In particular, if  $\rho(\mathbf{Df}(\mathbf{x})) < 1$  for all  $\mathbf{x}$ , then  $\|\mathbf{Df}(\mathbf{x})\|_2 < 1$  everywhere, implying that infinitesimal perturbations contract uniformly and that the maximal Lyapunov exponent is negative. This relationship naturally motivates the common identification of transitions to chaos with a form of *spectral critical-*

*ity*, namely the excursion of eigenvalues of the Jacobian outside the unit circle.

Here we show that identifying the instability required for chaos with eigenvalue criticality is incomplete in dimensions  $d > 1$ . Spectral analysis captures only part of the stability landscape: the geometry of singular values and the non-normality of the operator provide additional independent routes to instability. In particular, chaotic dynamics can arise even when  $\rho(\mathbf{Df}(\mathbf{x})) < 1$  for *all* states  $\mathbf{x}$  visited by the trajectory, so that no spectral criticality occurs at any time. In this sense, chaos need not originate from eigenvalue crossing; it can emerge purely from geometric amplification mechanisms. We demonstrate this constructively by introducing an explicit three-dimensional discrete-time system, the *non-normal switching reinjection torus* (NNSRT) map on  $\Omega = \mathbb{T}^3$ , whose Jacobian is everywhere (almost) block-triangular and pointwise spectrally contracting, with spectral radius uniformly bounded away from unity. Its dynamics undergoes a transition from regular to chaotic behavior as a *non-normality index*  $K$  is increased while keeping the eigenvalues of the Jacobian, hence its spectral radius, fixed below 1. The mechanism exploits the transient growth characteristic of non-normal systems [10, 11]. Although each instantaneous Jacobian is spectrally stable, non-orthogonal eigenvectors allow short-time amplification measured by singular values. In the NNSRT, this amplification is not merely transient: an endogenous switching variable repeatedly *reinjects* trajectories into amplifying directions, thereby converting local transient growth into sustained instability and chaotic dynamics. Together these results establish a deterministic route to chaos controlled by non-normality and alternation of transiently unstable directions rather than by eigenvalue instability, thereby showing that non-

normal amplification can mimic and even replace spectral criticality in the onset of complex dynamics [12].

*Spectral expansion as the classical route to chaos.* We begin by recalling the standard mechanism underlying chaotic dynamics in low-dimensional systems [3]. In one dimension, and more generally for normal Jacobians, Lyapunov instability is directly controlled by the instantaneous eigenvalues, so that spectral expansion and Lyapunov instability coincide. Consider a  $C^1$  map  $\mathbf{x}_{n+1} = \mathbf{f}(\mathbf{x}_n)$ ,  $\mathbf{x}_n \in \Omega \subset \mathbb{R}^d$ , with  $\Omega$  bounded and forward invariant. Let  $\mathbf{Df}(\mathbf{x})$  denote the Jacobian, the maximal Lyapunov exponent is

$$\lambda_{\max}(x_0) = \limsup_{n \rightarrow \infty} \frac{1}{n} \log \|\mathbf{Df}(\mathbf{x}_{n-1}) \cdots \mathbf{Df}(\mathbf{x}_0)\|. \quad (1)$$

In one dimension, the Jacobian reduces to the scalar derivative  $f'(x)$  and  $\lambda(x_0) = \lim_{n \rightarrow \infty} \frac{1}{n} \sum_{k=0}^{n-1} \log |f'(x_k)|$ . Hence exponential sensitivity requires  $|f'(x_k)| > 1$  on average along trajectories [8, 9]. In particular, if  $|f'(x)| < 1$  for all  $x \in \Omega$ , then  $\lambda_{\max} < 0$  and chaos is impossible. Spectral contraction and norm contraction coincide identically. For  $d > 1$ , submultiplicativity yields

$$\|\mathbf{Df}(\mathbf{x}_{n-1}) \cdots \mathbf{Df}(\mathbf{x}_0)\| \leq \prod_{k=0}^{n-1} \|\mathbf{Df}(x_k)\|. \quad (2)$$

When each  $\mathbf{Df}(\mathbf{x})$  is *normal*,  $\mathbf{Df}(\mathbf{x})\mathbf{Df}(\mathbf{x})^\dagger = \mathbf{Df}(\mathbf{x})^\dagger\mathbf{Df}(\mathbf{x})$ , then it is diagonalizable in an orthonormal basis and  $\|\mathbf{Df}(x)\| = \rho(\mathbf{Df}(\mathbf{x}))$ , which is the spectral radius of the Jacobian. Therefore, if  $\rho(\mathbf{Df}(\mathbf{x})) < 1$  for all  $\mathbf{x} \in \Omega$ , then  $\lambda_{\max} < 0$ . Thus, in one dimension and, more generally, for normal Jacobians, Lyapunov instability is entirely controlled by eigenvalues: sustained chaos requires spectral expansion along portions of the trajectory. In this setting, multiplicative growth cannot exceed what is dictated by the eigenvalues, and the presence of additional dimensions does not introduce qualitatively new instability mechanisms as long as the orthogonality of eigenvectors is preserved.

*The Non-Normal Shear-Rotation Torus Map (NNSRT) Map.* To demonstrate constructively that chaos can coexist with everywhere spectral contraction in autonomous deterministic systems, we introduce the following three-dimensional discrete-time map:

$$\begin{aligned} \mathbf{x}_{n+1} &= \mathbf{A}(z_n)\mathbf{x}_n \pmod{1}, \\ z_{n+1} &= \alpha_z z_n + \epsilon g(\mathbf{x}_n) \pmod{1}, \end{aligned} \quad (3)$$

where  $\mathbf{x}_n \in \mathbb{T}^2$ ,  $z_n \in \mathbb{T}$ ,  $0 < \alpha_z < 1$  and  $0 < \epsilon < 1$ . The  $2 \times 2$  matrix  $\mathbf{A}(z)$  is defined as

$$\mathbf{A}(z) = \mathbf{R}(\omega z) \mathbf{A} \mathbf{R}(\omega z)^T, \quad \omega = \frac{\pi}{2} \quad (4)$$

where  $\mathbf{R}(\theta)$  is a rotation matrix and the non-normal  $2 \times 2$  matrix  $\mathbf{A}$  is

$$\mathbf{A} = \begin{pmatrix} \alpha & \beta\kappa \\ \beta\kappa^{-1} & \alpha \end{pmatrix}, \quad (5)$$

with  $\alpha, \beta > 0$ . The variable  $z$  and its dynamics control the rotation of  $\mathbf{A}(z)$ , whose eigenvectors switch rapidly when  $z$  jumps from values close to 0 to values close to 1. Piecewise-linear and switched linear systems play a central role in control theory and power electronics [13, 14], where products of stable linear operators are applied in alternation. Even when each subsystem is individually stable, switching can induce instability, a phenomenon well documented in the theory of switched systems [13, 14].

The eigenvalues of  $\mathbf{A}$  and  $\mathbf{A}(z)$  are  $\lambda_{\pm} = \alpha \pm \beta$ , so that the spectral radius is  $\rho(\mathbf{A}) = \alpha + \beta$ . The parameter  $\kappa \geq 1$  controls the departure from normality. For  $\kappa = 1$ , the matrix is symmetric and therefore normal. For  $\kappa > 1$ , eigenvectors are non-orthogonal and  $\mathbf{A}$  is non-normal. It is convenient to introduce the *non-normal index*

$$K = \frac{\kappa - \kappa^{-1}}{2}, \quad (6)$$

which vanishes in the normal limit and increases monotonically with eigenvector non-orthogonality [12].

Equations (3)-(5) define an autonomous, bounded map in which the planar state  $\mathbf{x}_n \in \mathbb{T}^2$  is advanced by a non-normal linear operator  $\mathbf{A}(z_n)$ , while the internal variable  $z_n \in \mathbb{T}$  contracts (rate  $\alpha_z$ ) and intermittently triggers near- $\pi/2$  reorientations of  $\mathbf{A}(z)$ . The control parameter is the non-normality index  $K$  (at fixed eigenvalues of the core matrix  $\mathbf{A}$ ). Unless stated otherwise, we use the baseline parameters  $\alpha = 0.7$ ,  $\beta = 0.2$ , which ensures  $\rho(\mathbf{A}) = \alpha + \beta = 0.9 < 1$ ,  $\alpha_z = 0.5$ , and  $\epsilon = 10^{-3}$  with  $g(x, y) = x + y - 1$  used in the simulations. Results remain robust for a large set of functions  $g(x, y)$ .

*Transition to Chaos.* Figs. 1-3 provide a three-way confirmation of the non-normal route to chaos: attractor broadening, positive Lyapunov exponent, and attractor fractalization, all occurring while the Jacobian eigenvalues remain uniformly inside the unit disk. Computational details are given in Sec. S2 of the Supplemental Material.

Figure 1 visualizes the long-time dynamics through coordinate-wise maxima  $x_{\max}$ ,  $y_{\max}$  and  $z_{\max}$  versus  $K/K_c$ , where  $K_c$  is defined below by condition (8). For  $K/K_c < 1$ , panels (a)-(b) display the cross-sections respectively along the  $x$  and  $y$  coordinates of discrete periodic orbits of finite periods. As  $K/K_c$  reaches unity, the attractor bifurcates to exhibit a thick structure with dense bands for  $K/K_c > 1$ . Panel (c) highlights the dynamics of the maximum  $z_{\max}$  of the third variable, which acts as an endogenized switch:  $z_{\max}$  remains largely confined to a small set of values, consistent with strong contraction in  $z$  punctuated by rare modulo-induced jumps.

Figure 2 isolates the central signature of the transition. As  $K/K_c$  increases, the maximal Lyapunov exponent becomes positive while the spectral radius of the Jacobian remains strictly below unity, showing that chaos emerges from non-normal amplification rather than eigenvalue in-

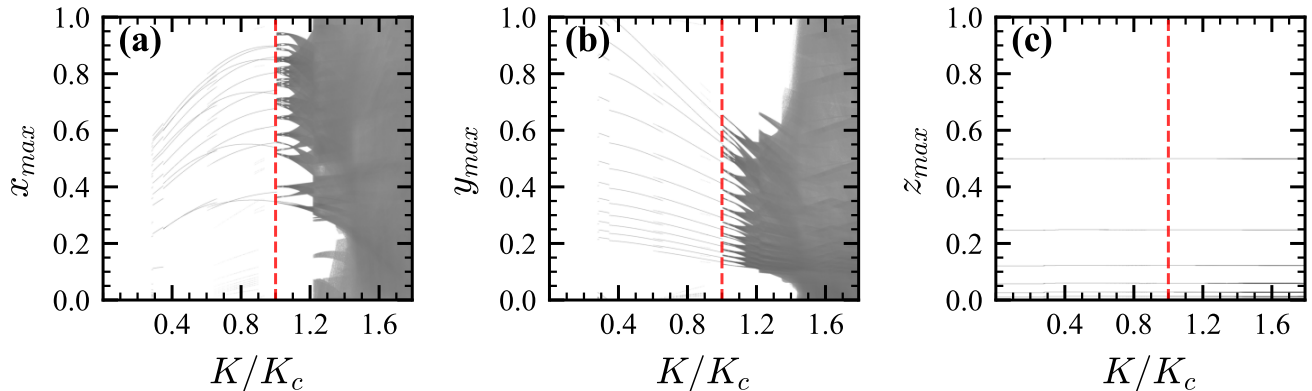


FIG. 1. Bifurcation portraits of the NNSRT map (3)-(5) shown through coordinate-wise maxima  $x_{\max}$  (a),  $y_{\max}$  (b), and  $z_{\max}$  (c) versus the normalised non-normality index  $K/K_c$  for  $\alpha = 0.7$ ,  $\beta = 0.2$ ,  $\alpha_z = 0.5$ , and  $\epsilon = 10^{-3}$ . The vertical dashed line marks the analytically predicted threshold  $K/K_c = 1$ .

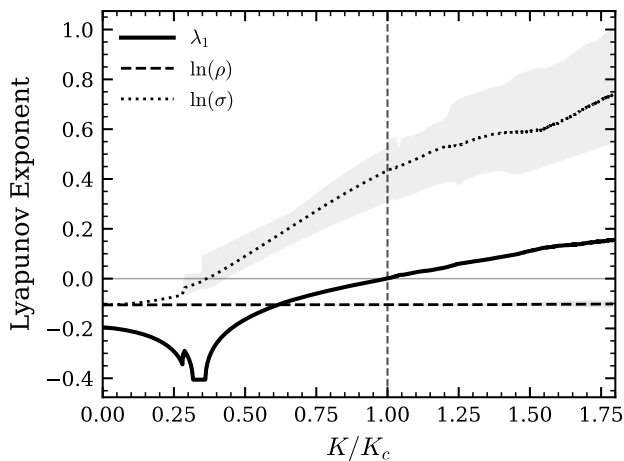


FIG. 2. Transition to chaos without spectral criticality for the dynamical system (3)-(5) with the same parameter values as in Fig. 1. Solid line: maximal Lyapunov exponent  $\lambda_1$  versus  $K/K_c$ . Dashed line:  $\ln(\rho)$ , where  $\rho$  is the spectral radius of the Jacobian  $\mathbf{Df}(\mathbf{x}_n, z_n)$  along the trajectory, (pointwise spectral contraction). Dotted line:  $\ln(\sigma)$ , where  $\sigma$  is the largest singular value of  $\mathbf{Df}(\mathbf{x}_n, z_n)$ , quantifying transient amplification enabled by non-normality; the shaded band indicates its variability along the orbit. The vertical line marks  $K = K_c$  at which  $\lambda_1$  crosses zero: chaos emerges while eigenvalues remain uniformly inside the unit disk.

stability. Crucially, the trajectory-wise spectral diagnostic  $\ln(\rho)$  (logarithm of the spectral radius of the Jacobian in dashed line) remains strictly negative and constant, taking the value  $\ln(0.9) \approx -0.15$  for all values of  $K/K_c$ , ensuring the persistence of pointwise spectral contraction over the whole spatial domain in the chaotic regime. In contrast, the singular-value diagnostic  $\ln(\sigma)$  (logarithm of the largest singular value of the Jacobian

in dotted line, with its uncertainty band) grows substantially with  $K/K_c$  and becomes positive, reflecting the increasing availability of transient amplification due to eigenvector non-orthogonality. The coexistence of  $\lambda_1 > 0$  with  $\ln(\rho) < 0$  demonstrates that the transition is controlled by non-normal transient growth plus reinjection, not by spectral criticality.

Fig. 3 provides a third diagnostic by showing how the fractal dimension of the attractor evolves with  $K/K_c$ . The box-counting dimension in  $(x, y, z)$  space,  $D_0^{xyz}$ , increases sharply across the transition, indicating the emergence and thickening of a strange attractor as non-normal amplification becomes dominant. Estimates based on the correlation dimension and the Kaplan–Yorke dimension show consistent behavior, supporting the same conclusion. For  $K/K_c < 1$ , the dimensions remain equal to 0, as expected for discrete periodic attractors. At  $K/K_c = 1$ , the fractal dimensions jump to values between 0 and 1, and then increase beyond 1 as  $K/K_c$  grows, consistent with the emergence of a fractal chaotic set.

*Non-Normal Mechanism for Chaos.* Chaos in the NNSRT map results from the interplay of two mechanisms. First, although each instantaneous Jacobian is spectrally stable, the non-orthogonality of its eigenvectors permits short-time amplification quantified by the singular values. Second, this transient amplification becomes recurrent through rotations of the map in the  $(x, y)$  plane driven by feedback from the third variable  $z$ . These rotations repeatedly switch the directions of transient amplification and reinject trajectories into them, converting local transient growth into sustained instability and chaotic dynamics. Because the map is everywhere spectrally contracting as the spectral radius of the Jacobian remains strictly smaller than one at all points, chaos emerges from the competition between this average contracting tendency and the transient amplification

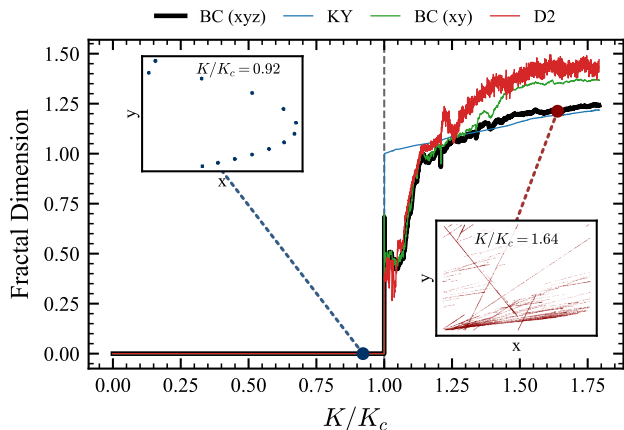


FIG. 3. Fractal-dimension diagnostics of the attractor versus the normalised non-normal index  $K/K_c$  for the dynamical system (3)-(5) with the same parameter values as in Fig. 1. The thick black curve shows the box-counting fractal dimension BC(xyz) of the attractor in the  $(x, y, z)$  space, while the colored curves show the Kaplan-Yorke dimension (KY), the Box-Counting fractal dimension BC(xy) of the projection of the attractor in the  $(x, y)$  plane, and the correlation dimension  $D_2$ . Insets show representative  $(x, y)$  projections of the attractor below ( $K/K_c = 0.92$ ) and above ( $K/K_c = 1.64$ ) the transition.

enabled by non-normality and made recurrent by the alternating amplifying directions. In other words, the dynamics reflect the balance between shrinking eigenvalues and amplifying singular values, with the rotations ensuring that the transiently amplifying directions are repeatedly revisited. In the absence of these rotations, spectral contraction would suppress any sustained instability and chaos would not occur.

In the NNSRT system (3), the strength of the rotations is controlled by parameter  $\epsilon$ . For  $\epsilon = 0$ , the  $z$ -dynamics contracts exponentially to the fixed point  $z = 0$ , the rotation matrix freezes to the identity and the long-term dynamics in the  $(x, y)$  plane converges to the origin. For  $\epsilon \neq 0$ , the term  $\epsilon g(\mathbf{x}_n)$  leads  $z_n$  to intermittently jump from values close to 0 to values close to 1. After a jump to  $z_n \approx 1$ ,  $z_{n+k}$  relaxes deterministically according to  $z_{n+k} \approx \alpha_z^{k-1}$  until it again becomes of order  $\epsilon$  and another jump becomes possible. Note that, for  $\epsilon\kappa \ll 1$ , the coupling between  $z$  and  $x + y$  remains perturbative and the  $z$ -dynamics is an almost smooth exponential relaxation between rare jump events.

The consequence of these jumps is to generate sudden rotations of the linear operator  $\mathbf{A}(z)$  by angles close to  $\pi/2$ . These abrupt reorientations repeatedly redirect the state vector into the non-orthogonal amplifying direction of  $\mathbf{A}$ . Between these reinjections, contraction dominates. The dynamics therefore alternates between (i) phases of contraction governed by  $\alpha_z$  along the  $z$ -dimension and by the eigenvalues  $\lambda_{\pm} = \alpha \pm \beta < 1$  of  $\mathbf{A}(z)$  in the  $(x, y)$

plane, (ii) brief episodes of non-normal amplification triggered by the rotations presenting the dynamics along the instantaneous amplification direction, and (iii) modulo-1 reinjections that maintain boundedness of the trajectory.

To a first approximation, an analytical proxy to determine the critical non-normality threshold  $K_c$  for the onset of chaos is obtained by considering that the eventual long-term behavior is governed by the two-step product

$$\lambda \approx \frac{1}{2} \log \|\mathbf{A}(0)\mathbf{A}(1)\|, \quad (7)$$

which depends only on the singular structure of  $\mathbf{A}$ . The critical threshold  $K_c$  is then defined as the value of  $K$  for which this approximate Lyapunov exponent vanishes,

$$\frac{1}{2} \log \|\mathbf{A}(0)\mathbf{A}(1)\| = 0 \iff \|\mathbf{A}(0)\mathbf{A}(1)\| = 1. \quad (8)$$

In general, the non-normal threshold  $K_c$  for the onset of chaos depends subtly on the structure of the map and on the interplay between its overall contraction properties, its degree of non-normality, and the manner in which transient amplification directions are sampled along the trajectory.

Maximal transient non-normal amplification is obtained when the rotational jumps satisfy  $\mathbf{A}(1) \approx \mathbf{A}(0)^T$ . In this limit,  $\mathbf{A}(0)\mathbf{A}(1) = \mathbf{A}(0)\mathbf{A}(0)^T$ , which is symmetric positive semidefinite and its norm is equal to its spectral radius  $\rho(\mathbf{A}(0)\mathbf{A}(0)^T) = \|\mathbf{A}\|^2 = \sigma_{\max}(\mathbf{A})^2$ , the square of the maximum singular value of  $\mathbf{A}$ . Although  $\rho(\mathbf{A}) \leq \|\mathbf{A}\|$ , for sufficiently strong non-normality ( $K$  sufficiently large) [10, 11], it is possible to have  $\rho(\mathbf{A}) < 1$  with  $\sigma_{\max}(\mathbf{A}) = \|\mathbf{A}\| > 1$ , and the two-step product expands even though each factor is spectrally contracting. The spectral radius no longer controls multiplicative growth. When all eigenvalues lie strictly inside the unit disk, certain perturbations can experience short-time amplification. This classical transient growth is central in hydrodynamic stability theory, where spectrally stable shear flows may exhibit large finite-time growth that triggers nonlinear transition to turbulence [11, 15].

To illustrate how non-normality can overcome spectral contraction, consider the minimal deterministic switching map

$$\mathbf{x}_{n+1} = \begin{cases} \mathbf{A}\mathbf{x}_n & (\text{mod } 1), \quad g(\mathbf{x}_n) > 0, \\ \mathbf{A}^T\mathbf{x}_n & (\text{mod } 1), \quad g(\mathbf{x}_n) \leq 0, \end{cases} \quad (9)$$

where  $\rho(\mathbf{A}) < 1$  and  $\sigma_{\max}(\mathbf{A}) > 1$ . The modulo operation ensures reinjection into a bounded domain. When alternation between the two branches occurs sufficiently often, the leading contribution to the Lyapunov exponent becomes  $\lambda \approx \frac{1}{2} \log \rho(\mathbf{A}^T\mathbf{A}) = \log \sigma_{\max}(\mathbf{A})$ , showing the enhancing effect of non-normality on  $\lambda$  beyond the spectral radius contribution  $\log(\rho(\mathbf{A}))$ . Thus, exponential growth occurs whenever  $\sigma_{\max}(\mathbf{A}) > 1$  despite spectral contraction ( $\log(\rho(\mathbf{A})) < 0$ ) at every step.

For the non-normal matrix  $\mathbf{A}$  defined in Eq. (5), the maximal singular value increases with the non-normality index  $K$  as  $\log \sigma_{\max}(\mathbf{A}) = \log(\rho(\mathbf{A})) + \frac{\beta}{2\alpha} K^2 + O(K^4)$ . At fixed spectral radius  $\rho(\mathbf{A}) = \alpha + \beta$ , a transition from contraction to amplification therefore occurs when  $\sigma_{\max}(\mathbf{A}) = 1$ , which defines a critical non-normality threshold  $K_c = \frac{1}{2\beta} \sqrt{(1 - \lambda_+^2)(1 - \lambda_-^2)} \approx \left[ \frac{2\alpha}{\beta} \ln\left(\frac{1}{\rho(\mathbf{A})}\right) \right]^{1/2}$ . Thus increasing eigenvector non-orthogonality alone can compensate for spectral contraction and produce global instability (see SM).

The non-normal route to chaos identified here is closely related to the classical *Perron effect* or *Perron-type instability* [16] known in nonautonomous dynamical systems. Consider a time-varying linear system  $\dot{\mathbf{x}} = \mathbf{A}(t)\mathbf{x}$  with continuous  $\mathbf{A}(t)$ . Perron showed that it is possible for all instantaneous eigenvalues of  $\mathbf{A}(t)$  to have negative real parts for every  $t$ , suggesting pointwise stability, while the fundamental matrix nevertheless grows exponentially so that the origin is unstable [16]. In such systems, the long-term growth is governed not by the instantaneous spectrum of  $\mathbf{A}(t)$  but by properties of the evolution operator, typically characterized by Lyapunov exponents or the Sacker–Sell spectrum [17, 18]. This illustrates a fundamental limitation of spectral diagnostics in nonautonomous systems: instantaneous eigenvalues alone do not determine stability unless additional structural conditions (such as commutativity or normality) are satisfied.

More generally, discrete-time systems with time-dependent linear operators  $\mathbf{x}_{n+1} = \mathbf{A}_n \mathbf{x}_n$  are governed by multiplicative growth rates determined by the product of the matrices, analogous to Lyapunov or Floquet exponents. Instability may therefore arise from the product structure itself, even when  $\rho(\mathbf{A}_n) < 1$  for all  $n$  [19]. This perspective is closely related to the concept of *exponential dichotomy* in nonautonomous stability theory [17], which characterizes stability through the growth properties of the evolution operator rather than through instantaneous eigenvalues.

The mechanism presented here can be viewed as a deterministic analogue of this Perron-type instability driven by eigenvector geometry rather than eigenvalue instability. In the NNSRT map, the explicit time dependence of  $\mathbf{A}_n$  is replaced by the autonomous evolution of the third variable  $z$ , which controls the matrix  $\mathbf{A}(z)$ . The dynamics of  $z$  generates the sequence of matrices applied along the trajectory, effectively endogenizing the switching mechanism while preserving uniform spectral contraction. In this way, the system realizes within an autonomous smooth map the same multiplicative mechanism that underlies Perron-type instability.

Our results clarify and extends several known phenomena. In hydrodynamic stability, subcritical transition arises from transient growth in spectrally stable flows

[11, 15]. In switched and hybrid control systems, products of individually stable operators may generate instability [13, 14]. In multiplicative stochastic processes, Lyapunov instability may occur without eigenvalue instability [19]. Our work shows that this principle persists in fully deterministic, autonomous, bounded nonlinear dynamics: non-normality alone can organize a genuine transition to chaos.

- 
- [1] E. N. Lorenz, Deterministic nonperiodic flow, *Journal of the Atmospheric Sciences* **20**, 130 (1963).
  - [2] S. Smale, Differentiable dynamical systems, *Bulletin of the American Mathematical Society* **73**, 747 (1967).
  - [3] E. Ott, *Chaos in Dynamical Systems*, 2nd ed. (Cambridge University Press, 2002).
  - [4] S. H. Strogatz, *Nonlinear Dynamics and Chaos* (Westview Press, 2015).
  - [5] M. J. Feigenbaum, Quantitative universality for a class of nonlinear transformations, *Journal of Statistical Physics* **19**, 25 (1978).
  - [6] Y. Pomeau and P. Manneville, Intermittent transition to turbulence in dissipative dynamical systems, *Communications in Mathematical Physics* **74**, 189 (1980).
  - [7] D. Ruelle and F. Takens, On the nature of turbulence, *Communications in Mathematical Physics* **20**, 167 (1971).
  - [8] R. L. Devaney, *An Introduction to Chaotic Dynamical Systems*, 2nd ed. (Westview Press, 2003).
  - [9] A. Katok and B. Hasselblatt, *Introduction to the Modern Theory of Dynamical Systems*, *Encyclopedia of Mathematics and its Applications*, Vol. 54 (Cambridge University Press, 1995).
  - [10] L. N. Trefethen and M. Embree, *Spectra and Pseudospectra: The Behavior of Nonnormal Matrices and Operators* (Princeton University Press, 2005).
  - [11] P. J. Schmid, Nonmodal stability theory, *Annual Review of Fluid Mechanics* **39**, 129 (2007).
  - [12] V. Troude, S. Lera, K. Wu, and D. Sornette, *Illusions of criticality: Crises without tipping points* (2025), [arXiv:2412.01833 \[nlin.CD\]](https://arxiv.org/abs/2412.01833).
  - [13] D. Liberzon, *Switching in Systems and Control* (Birkhäuser, 2003).
  - [14] R. A. DeCarlo, M. S. Branicky, S. Pettersson, and B. Lennartson, Perspectives and results on the stability and stabilizability of hybrid systems, *Proceedings of the IEEE* **88**, 1069 (2000).
  - [15] T. Gebhardt and S. Grossmann, Chaos transition despite linear stability, *Physical Review E* **50**, 3705 (1994).
  - [16] O. Perron, Die stabilitätsfrage bei differentialgleichungen, *Mathematische Zeitschrift* **32**, 703 (1930).
  - [17] W. A. Coppel, *Dichotomies in Stability Theory*, *Lecture Notes in Mathematics*, Vol. 629 (Springer, 1978).
  - [18] R. J. Sacker and G. R. Sell, A spectral theory for linear differential systems, *Journal of Differential Equations* **27**, 320 (1978).
  - [19] A. Crisanti, G. Paladin, and A. Vulpiani, *Products of Random Matrices in Statistical Physics*, *Springer Series in Solid-State Sciences*, Vol. 104 (Springer, 1993).
  - [20] G. Benettin, L. Galgani, A. Giorgilli, and J.-M. Strelcyn,

Lyapunov characteristic exponents for smooth dynamical systems and for hamiltonian systems; a method for computing all of them. part 1: Theory, *Meccanica* **15**, 9 (1980).

- [21] G. Benettin, L. Galgani, A. Giorgilli, and J.-M. Strelcyn, Lyapunov characteristic exponents for smooth dynamical systems and for hamiltonian systems; a method for computing all of them. part 2: Numerical application, *Meccanica* **15**, 21 (1980).
- [22] J. L. Kaplan and J. A. Yorke, Chaotic behavior of multi-dimensional difference equations, in *Functional Differential Equations and Approximation of Fixed Points*, Lecture Notes in Mathematics, Vol. 730, edited by H.-O. Peitgen and H.-O. Walther (Springer, Berlin, Heidelberg, 1979) pp. 204–227.
- [23] P. Frederickson, J. L. Kaplan, E. D. Yorke, and J. A. Yorke, The liapunov dimension of strange attractors, *Journal of Differential Equations* **49**, 185 (1983).
- [24] K. Falconer, *Fractal Geometry: Mathematical Foundations and Applications*, 3rd ed. (John Wiley & Sons, 2014).
- [25] P. Grassberger and I. Procaccia, Characterization of strange attractors, *Physical Review Letters* **50**, 346 (1983).
- [26] P. Grassberger and I. Procaccia, Measuring the strangeness of strange attractors, *Physica D: Nonlinear Phenomena* **9**, 189 (1983).

## Supplementary Material

### MODE SWITCHING MAP

To understand how this lead to chaos, let us consider the minimal deterministic switching map

$$\mathbf{x}_{n+1} = \begin{cases} \mathbf{A}\mathbf{x}_n \pmod{1}, & g(\mathbf{x}_n) > 0, \\ \mathbf{A}^T\mathbf{x}_n \pmod{1}, & g(\mathbf{x}_n) \leq 0, \end{cases} \quad (10)$$

where  $\rho(\mathbf{A}) < 1$  and  $\sigma_{\max}(\mathbf{A}) > 1$ . The modulo operation ensures reinjection into a bounded domain. When alternation between  $g(\mathbf{x}_n) > 0$  and  $g(\mathbf{x}_n) \leq 0$  occurs sufficiently often, the leading contribution to the Lyapunov exponent is  $\lambda \approx \frac{1}{2} \log \rho(\mathbf{A}^T\mathbf{A}) = \log \sigma_{\max}(\mathbf{A})$ . Therefore  $\lambda > 0$  whenever  $\sigma_{\max}(\mathbf{A}) > 1$ , despite  $\rho(\mathbf{A}) < 1$  at every step. This simple map illustrates how non-normality converts short-time amplification into sustained exponential growth in the presence of alternation between the two eigendirections. These considerations show that the key object of interest is the maximum singular value of matrix  $\mathbf{A}$ , such that

$$\mathbf{A} = \begin{pmatrix} \alpha & \beta\kappa \\ \beta/\kappa & \alpha \end{pmatrix}, \quad \alpha, \beta > 0. \quad (11)$$

A direct computation gives  $\sigma_{\max}(\mathbf{A}) = \sqrt{S + \sqrt{S^2 - (\alpha^2 - \beta^2)^2}}$ , where  $S = \alpha^2 + \beta^2 + 2\beta^2K^2$ .

Expanding in powers of  $K$ , we find

$$\log \sigma_{\max}(\mathbf{A}) = \log(\rho(\mathbf{A})) + \frac{\beta}{2\alpha}K^2 + O(K^4). \quad (12)$$

Expression (12) illustrates how non-normality can significantly increase the maximum singular value above the spectral radius: for a fixed  $\rho(\mathbf{A}) = \alpha + \beta$ ,  $\sigma_{\max}(\mathbf{A})$  grows with  $K$ . For the special map (10), the non-normality threshold for the onset of chaos is given by the condition  $\sigma_{\max}(\mathbf{A}) = 1$ , which yields  $K_c = \frac{1}{2\beta} \sqrt{(1 - \lambda_+^2)(1 - \lambda_-^2)} \approx \left[ \frac{2\alpha}{\beta} \ln(1/\rho(\mathbf{A})) \right]^{\frac{1}{2}}$ . The smaller the spectral radius  $\rho(\mathbf{A})$ , that is, the more strongly contracting the map, the greater the degree of non-normality required to produce chaos, so that transient non-normal amplification events can compensate for the overall contraction. Thus, even for spectrally contracting maps, a transition from net contraction to global amplification can occur purely through increasing eigenvector non-orthogonality. This identifies non-normality as an independent control parameter, effectively decoupled from eigenvalue instability.

### METHODOLOGY

All numerical diagnostics were generated with Python, which performs a sweep over the non-normality index  $K/K_c$  and computes the quantities reported in Fig. 2 and 3 of the manuscript. They are the largest Lyapunov exponent  $\lambda_1$ , the Kaplan–Yorke dimension  $D_{KY}$ , two occupied-bin box-counting estimates in  $(x, y)$  and  $(x, y, z)$ , and a correlation-dimension estimate  $D_2$ . For each parameter value  $K/K_c$ , we computed dynamical and geometric diagnostics from long post-transient trajectories of the three-dimensional torus map

$$\mathbf{X}_{n+1} = F_K(\mathbf{X}_n), \quad \mathbf{X}_n = (x_n, y_n, z_n) \in [0, 1]^3.$$

Unless stated otherwise, the baseline parameter values are  $\alpha = 0.7$ ,  $\beta = 0.2$ ,  $\alpha_z = 0.5$ ,  $\epsilon = 10^{-3}$ , and rotation scale  $\omega = \pi/2$  and using  $n_K = 5000$  evenly spaced values for parameters sweeps.

### Lyapunov spectrum

Let

$$J_n = DF_K(\mathbf{X}_n)$$

denote the Jacobian matrix evaluated along a trajectory  $\{\mathbf{X}_n\}$ . The  $N$ -step tangent propagator is

$$M_N(\mathbf{X}_0) = J_{N-1}J_{N-2}\cdots J_0.$$

The Lyapunov exponents are the asymptotic logarithmic growth rates of the singular values of  $M_N$ ,

$$\lambda_i = \lim_{N \rightarrow \infty} \frac{1}{N} \log \sigma_i(M_N(\mathbf{X}_0)), \quad \lambda_1 \geq \lambda_2 \geq \lambda_3,$$

for typical initial conditions on the invariant set [20, 21]. We used the standard Benettin–QR procedure. After discarding an initial transient of  $N_{\text{burn}}^{(\lambda)} = 2 \times 10^4$  iterates, we initialized a random orthonormal basis  $Q_0 \in \mathbb{R}^{3 \times 3}$  and iterated

$$Z_n = J_n Q_n, \quad Z_n = Q_{n+1} R_n,$$

where  $Q_{n+1}$  is orthonormal and  $R_n$  is upper triangular. The finite-time Lyapunov exponents are then estimated as

$$\hat{\lambda}_i(N) = \frac{1}{N} \sum_{n=0}^{N-1} \log |(R_n)_{ii}|, \quad i = 1, 2, 3.$$

We used  $N_{\text{iter}}^{(\lambda)} = 6 \times 10^4$  accumulation iterates for each value of  $K$ , and the resulting three exponents were sorted in descending order before further post-processing. The quantity plotted in the main text is the largest exponent  $\lambda_1$ . Its sign provides the standard asymptotic classification:  $\lambda_1 < 0$  indicates stability and convergence toward a regular attracting fixed point or periodic set,  $\lambda_1 = 0$  marks neutral growth, and  $\lambda_1 > 0$  signals sensitive dependence on initial conditions and hence chaos. For clarity, we note that local one-step Jacobian diagnostics are distinct from Lyapunov exponents. Along the same orbit, one may define the instantaneous spectral radius and singular values.

### Kaplan–Yorke dimension

From the full Lyapunov spectrum  $(\lambda_1, \lambda_2, \lambda_3)$ , we computed the Kaplan–Yorke dimension

$$D_{\text{KY}} = j + \frac{\lambda_1 + \dots + \lambda_j}{|\lambda_{j+1}|},$$

where  $j$  is the largest integer such that

$$\sum_{i=1}^j \lambda_i \geq 0 \quad \text{and} \quad \sum_{i=1}^{j+1} \lambda_i < 0$$

[22, 23]. This quantity is a Lyapunov-based estimate of attractor dimension, derived from asymptotic tangent-space stretching rates rather than from direct geometric coverings. In the present three-dimensional setting, the observed values of  $D_{\text{KY}}$  lie between 1 and 2 throughout the chaotic regime, indicating an effectively filamentary strange attractor embedded in three-dimensional phase space. We emphasize, however, that  $D_{\text{KY}}$  is not identical to a box-counting or correlation dimension; it is a complementary spectrum-based estimator.

### Occupied-bin box-counting estimates

To quantify the geometric complexity of the sampled attractor directly, we estimated finite-resolution box-

counting dimensions in both the projected plane  $(x, y)$  and the full state space  $(x, y, z)$ . For a compact set  $A$ , the box-counting dimension is

$$D_0(A) = \lim_{\varepsilon \rightarrow 0} \frac{\log N(\varepsilon)}{\log(1/\varepsilon)},$$

where  $N(\varepsilon)$  is the minimum number of boxes of side length  $\varepsilon$  required to cover  $A$  [24]. Numerically, we used uniform grids on the unit torus. For a grid with  $m$  bins per coordinate direction, the box size is

$$\varepsilon = \frac{1}{m}.$$

For the  $(x, y)$  projection, we counted the number  $N_{xy}(m)$  of occupied boxes in an  $m \times m$  partition of  $[0, 1]^2$ . For the full attractor, we counted the number  $N_{xyz}(m)$  of occupied boxes in an  $m \times m \times m$  partition of  $[0, 1]^3$ . The corresponding finite-resolution dimension estimates were obtained as the least-squares slopes

$$D_{0,xy}^{(\text{est})} = \text{slope} \left[ \log N_{xy}(m) \text{ vs. } \log m \right],$$

$$D_{0,xyz}^{(\text{est})} = \text{slope} \left[ \log N_{xyz}(m) \text{ vs. } \log m \right].$$

Since  $\varepsilon = 1/m$ , these slopes are the direct finite-scale analogues of the standard box-counting definition.

For each  $K$ , we used 10 independent seeds, each generating a trajectory of length  $N_{\text{dim}} = 8 \times 10^4$  after a burn-in of  $N_{\text{burn}}^{(\text{dim})} = 2 \times 10^4$  iterates. The grid resolutions were

$$m \in \{32, 48, 64, 96, 128\}.$$

For each seed, we computed the slope separately, then reported the seed-averaged values and their dispersion. The curves labelled BC( $xy$ ) and BC( $xyz$ ) in the figure therefore represent finite-resolution occupied-bin scaling estimates, not exact  $\varepsilon \rightarrow 0$  limits. This distinction is important. In exact theory, the box-counting dimension is defined by an asymptotic limit. In numerics, the estimate depends on a restricted scaling range, finite trajectory length, and finite sampling density. For this reason, we interpret BC( $xy$ ) and BC( $xyz$ ) as robust geometric proxies rather than exact dimensions. BC( $xy$ ) quantifies the dimension of the projected attractor in the plane, whereas BC( $xyz$ ) quantifies the dimension of the sampled set in the full three-dimensional state space.

### Correlation dimension

As an additional, independent measure of fractal geometry, we computed the correlation dimension  $D_2$  using a Grassberger–Procaccia-type estimator [25, 26]. For a point cloud  $\{\mathbf{X}_i\}_{i=1}^M \subset \mathbb{R}^d$ , the correlation sum is

$$C(r) = \frac{2}{M(M-1)} \sum_{1 \leq i < j \leq M} \Theta(r - \|\mathbf{X}_i - \mathbf{X}_j\|),$$

where  $\Theta$  is the Heaviside function. The correlation dimension is defined by

$$D_2 = \lim_{r \rightarrow 0} \frac{d \log C(r)}{d \log r}.$$

In our implementation,  $D_2$  was estimated only in the full  $(x, y, z)$  space. For each  $K$ , after a burn-in of  $N_{\text{burn}}^{(2)} = 2.5 \times 10^4$  iterates, we collected a trajectory of length  $N_2 = 2 \times 10^4$ . From this trajectory, we selected without replacement a random subset of

$$M = 1500$$

points, and computed the Euclidean pairwise distances among these points. The empirical correlation sum  $C(r)$  was then evaluated over 28 logarithmically spaced radii

$$r \in [10^{-3}, 3 \times 10^{-1}].$$

Finally,  $D_2$  was estimated as the least-squares slope of  $\log C(r)$  versus  $\log r$  restricted to the intermediate scaling

window

$$10^{-3} \leq C(r) \leq 10^{-1}.$$

This exclusion of both very small and very large  $r$  suppresses undersampling noise at the smallest scales and saturation effects at the largest scales. As with the occupied-bin estimate, the computed  $D_2$  is a finite-sample proxy rather than an exact asymptotic limit. Moreover, in the present implementation we did not impose an explicit Theiler window; instead, temporal redundancy was reduced by random subsampling from a much longer orbit. Accordingly,  $D_2$  should be viewed as a corroborative measure of attractor complexity rather than as a single definitive dimension.

### Bifurcation

To generate the bifurcation-style portraits, we simulate a single long orbit for each  $K/K_c$  from a  $K/K_c$ -dependent but deterministic initial condition. After  $N_{\text{burn}}^{\text{bif}} = 20000$  burn-in iterates, we record  $N_{\text{col}}^{\text{bif}} = 1500$  successive values of  $x_n, y_n, z_n$ .